

Analytical study of wind-rain-induced cable vibration : 2DOF model

L.Y. Wang[†] and Y.L. Xu[‡]

*Department of Civil and Structural Engineering, The Hong Kong Polytechnic University,
Hung Hom, Kowloon, Hong Kong, China*

(Received October 18, 2002, Accepted July 14, 2003)

Abstract. Many investigations have been conducted to find out the reason behind wind-rain-induced cable vibration in cable-stayed bridges. A single-degree-of-freedom (SDOF) analytical model, which could capture main features of wind-rain-induced cable vibration, was recently presented by the writers. This paper extends the SDOF model to a 2DOF model by including the equation of motion of upper rivulet. The interaction between the upper rivulet and the cable is described in terms of nonlinear damping force, linear restoring force, and inertia force. The computed results using the 2DOF model are first compared with the results from simulated wind-rain tunnel tests, and the comparison is found satisfactory in general. The possible mechanisms of wind-rain-induced cable vibration are discussed and a parametric study is then conducted. Finally, the computed results using the 2DOF model are compared with those predicted by the SDOF model. The 2DOF model is found better than the SDOF model but the SDOF model is still acceptable for its simplicity.

Keywords: stay cable; cable vibration; wind; rain; moving rivulet; SDOF model; 2DOF model; comparison.

1. Introduction

Excessive and unanticipated vibration of stay cables has been observed in some cable-stayed bridges throughout the world, which often occurs under the simultaneous occurrence of wind and rain. Many studies have thus been conducted to find out the reason behind this new type of cable vibration and the measures for mitigating such a vibration. Hikami and Shiraishi (1988) conducted field measurements of stay cables subject to wind with and without rain and reproduced wind-rain-induced cable vibration in their simulated wind-rain tunnel tests. They concluded that the rivulet formed along the upper surface of a stay cable under the action of both wind and rain changed the original cable cross section and resulted in excessive cable vibration. Matsumoto *et al.* (1992) performed extensive wind-rain tunnel tests and pointed out that wind-rain-induced cable vibration was due to two major factors; one was the formation of upper rivulet and the other was the axial flow generated in the wake of an inclined cable. Matsumoto *et al.* (2001) also observed that even without upper rivulet, an inclined cable could vibrate significantly because of the fluid interaction between Karman vortex and axial vortex. They defined such a vibration as vortex-induced vibration of inclined cable at high wind velocity. Bosdogianni and Olivari (1996) compared wind tunnel

[†] PhD Student

[‡] Professor

results of cables with moving rivulet with those of the same cables but with fixed rivulet. They concluded that it was the presence of rivulet at a certain position and not the motion of rivulet that caused cable instability. However, Ruscheweyh (1999) stated that the movement of rivulet was the “trigger” for wind-rain-induced cable vibration and if the movement of rivulet could be stopped, rain-wind induced cable vibration would stop. Clearly, wind-rain-induced cable vibration is a complicated solid-fluid-wind interaction problem, and its mechanism is not well understood yet. Field measurements and observations of high quality are thus desirable and being carried out by researchers throughout the world, such as Zuo and Jones (2003) and Matsumoto *et al.* (2003).

Compared with the field measurements and the wind-rain-tunnel model tests, analytical studies on wind-rain-induced cable vibration are very limited. Yamaguchi (1990) presented a two-degree-of-freedom (2DOF) galloping model to describe wind-rain-induced cable vibration. In his model, the cable was modeled as a horizontal rigid cylinder only. He concluded that SDOF galloping theory might not be useful to explain the mechanism of wind-rain-induced cable vibration. Geurts and Staaldin (1999), however, presented an engineering approach to the same problem but based on the SDOF galloping theory. Recently, the writers presented a SDOF analytical model for describing the steady-state wind-rain-induced cable vibration including the full interaction between wind, rivulet and cable (Xu and Wang 2003). The SDOF model was then applied to some cable models tested in either a wind tunnel with fixed artificial rivulet or a wind-rain tunnel with moving rivulet. They found that the SDOF model could capture main features of wind-rain-induced cable vibration, such as velocity-restricted vibration and amplitude-restricted vibration. The occurrence of wind-rain-induced cable vibration was mainly because of alternating aerodynamic damping and/or aerodynamic force due to the interaction between rivulet, cable and wind. However, the motion of rivulet was assumed to be a known harmonic motion in the SDOF model, and accordingly only the steady-state wind-rain-induced cable vibration could be predicted.

In this paper, the SDOF model is extended to a 2DOF model by including the equation of motion of the upper rivulet. In the 2DOF model, the rotating motion of the rivulet around the central axis of the cable segment (cylinder) is considered together with the transverse motion of the inclined cylinder. The interaction between the upper rivulet and the cylinder is described in terms of nonlinear damping force, linear restoring force, and inertia force. The 4th-order Lunge-Kutta method provided in the MATLAB is used to solve the nonlinear equation of motion of the coupled wind-rivulet-cylinder system. The oscillation features of both the rivulet and the cylinder under wind are investigated. The computed results from the 2DOF model are compared with those obtained from the simulated wind-rain tunnel tests and those predicted by the SDOF model. Extensive parametric studies are performed and the possible mechanisms of wind-rain-induced cable vibration are sought.

2. 2DOF model

A rigid and uniform inclined cylinder is employed to represent a stay cable segment (see Fig. 1(a)). The inclination of the cylinder is denoted by angle α , and the yaw angle of the incident wind is designated by angle β . The cylinder is supposed to be supported by springs at its ends in the plane 1-5-7. The upper rivulet is assumed to uniformly distribute along the longitudinal axis of the cylinder and circumferentially vibrate over the surface of the cylinder. Turbulent effect and axial flow effect are not considered at this stage. The static position of the upper rivulet due to the mean wind when the cylinder is stationary is defined by angle θ_0 , and the dynamic angular displacement of the rivulet as the cylinder vibrates is designated by θ with reference to θ_0 (see Fig. 1(b)). Since

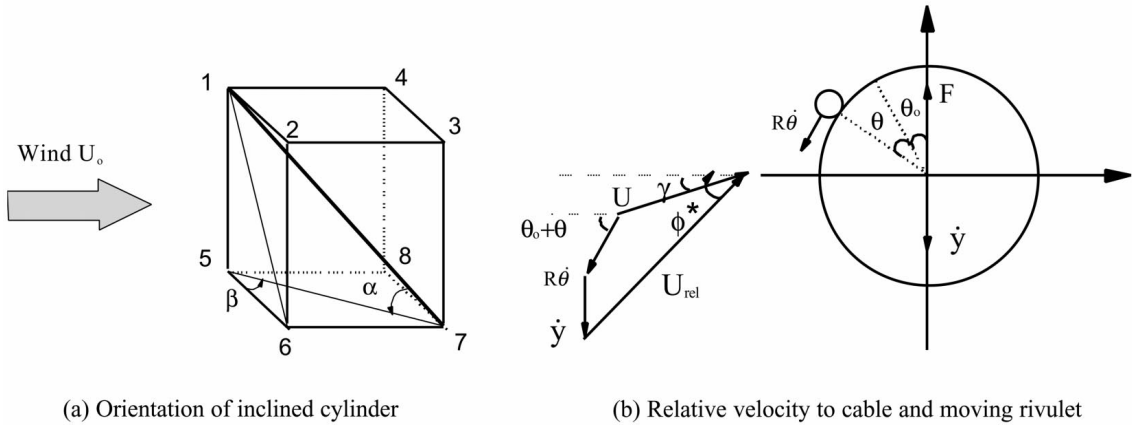


Fig. 1 Modeling of wind-rain-induced cable vibration

the cylinder is not perpendicular to the direction of the mean wind speed U_o , one needs to find the component of mean wind speed perpendicular to the cylinder, U , using the following equation.

$$U = U_o \sqrt{\cos^2 \beta + \sin^2 \alpha \sin^2 \beta} = U_o \sqrt{\sin^2 \alpha + \cos^2 \alpha \cos^2 \beta} \quad (1)$$

The angle of attack of the component U of the mean wind speed U_o is defined as γ , which indicates the stagnation point of incident wind on the surface of cylinder. The position of stagnation point depends on many factors such as the cross section of cylinder with rivulet, roughness of cylinder surface, wind turbulence, and cable motion. No experimental results are available to the writers at this stage with respect to the position of stagnation point on a stay cable with rivulet. Thus, the angle of attack in this study is selected as the ideal angle of attack multiplied by an influence factor ε .

$$\gamma = \varepsilon \sin^{-1} \left(\frac{\sin \sigma \sin \beta}{\sqrt{\cos^2 \beta + \sin^2 \alpha \sin^2 \beta}} \right) \quad (2)$$

When ε is set as 1, γ represents the ideal angle of attack for the cylinder without rivulet. When ε is selected as zero, it indicates that the position of stagnation point is the same as that on the cylinder without rivulet and yaw angle. In terms of the transverse vibration of the cylinder of velocity $\dot{y}(t)$ and the angular vibration of the upper rivulet of velocity $\dot{\theta}(t)$, the relative velocity of the mean wind U_{rel} to the cylinder with moving rivulet and the angle between the relative velocity and the horizontal axis ϕ^* can be found as follows:

$$U_{rel} = \sqrt{(U \cos \gamma + R \dot{\theta} \cos(\theta + \theta_o))^2 + (U \sin \gamma + \dot{y} + R \dot{\theta} \sin(\theta + \theta_o))^2} \quad (3)$$

$$\phi^* = \tan^{-1} \frac{U \sin \gamma + \dot{y} + R \dot{\theta} \sin(\theta + \theta_o)}{U \cos \gamma + R \dot{\theta} \cos(\theta + \theta_o)} \quad (4)$$

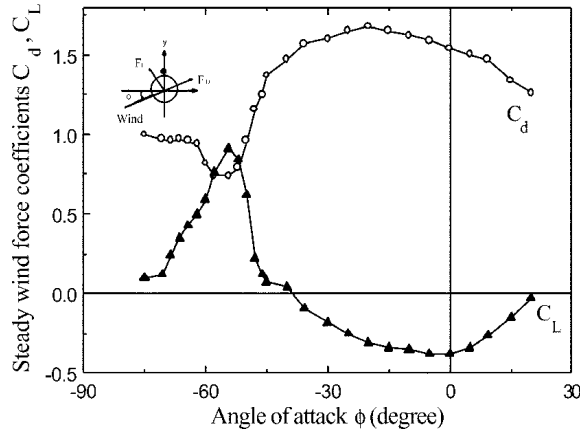


Fig. 2 Aerodynamic coefficients vs. wind angle of attack (Hikami and Shiraishi 1988)

The net vertical force on the cylinder per unit length in the y -direction is then

$$F = \frac{\rho D U_{rel}^2}{2} [C_L(\phi) \cos \phi^* + C_d(\phi) \sin \phi^*] \tag{5}$$

where ρ is the density of the air; D is the diameter of the cross-section of the cylinder; C_d is the drag coefficient; and C_L is the lift coefficient. The drag and lift coefficients of the cylinder with rigid rivulet measured from the wind tunnel tests are often expressed as the function of the angle ϕ defined in Fig. 2 (Hikami and Shiraishi 1988). The relationship between the angles ϕ^* and ϕ is given by

$$\phi = \phi^* - \theta - \theta_o = \frac{U \sin \gamma + \dot{y} + R \dot{\theta} \left[(\theta + \theta_o) - \frac{1}{6}(\theta + \theta_o)^3 \right]}{U \cos \gamma} - \theta - \theta_o \tag{6}$$

The expansion of the sine and cosine functions in Eq. (5) and the reservation of the linear terms of \dot{y} , θ and $\dot{\theta}$ only lead to

$$F_y = \frac{\rho D}{2} (\Gamma_1 R U_o \dot{\theta} + \Gamma_2 U_o \dot{y} + \Gamma_3 U_o^2 \theta) \tag{7}$$

where R is the radius of the cross-section of the cylinder; and Γ_1 , Γ_2 and Γ_3 are not only the function of the cable inclination, wind yaw angle, wind stagnation point, and the mean wind speed via the static position of rivulet but also the function of cable motion and rivulet motion which may change the values of drag coefficient and lift coefficient (Xu and Wang 2003).

In consideration that the cylinder structural damping is viscous and the cylinder mass is uniformly distributed, the dynamic equilibrium of the cylinder with the moving upper rivulet in the y -direction leads to the following equation of motion.

$$M \ddot{y} + C \dot{y} + K y + F_y = 0 \tag{8}$$

where M , C , and K are the mass, damping coefficient, and stiffness coefficient per unit length of the

cylinder. In Eq. (8), the component of the inertia force of the rivulet in the y -direction is neglected because it is very small compared with the inertia force of the cylinder in the y -direction.

For the upper rivulet, it is assumed that the mean wind force, the supporting force from the cylinder, and the gravity force on the rivulet all keep the rivulet in the static position θ_o . The dynamic equilibrium of the rivulet in the circumferential direction of the cylinder depends on the rivulet inertia force and the interacting force from the cylinder at the contacting surface with the rivulet. As the absolute acceleration of the rivulet is the superposition of the cylinder vertical acceleration at the contacting point and the acceleration of the rivulet relative to the cylinder, the acceleration of the rivulet in the tangential direction at the contacting point with the cylinder is given by $\ddot{y}\sin(\theta + \theta_o) + R\ddot{\theta}$. Besides the inertia force, the rivulet is subjected to turbulent wind force, aerodynamic damping force, restoring force due to water surface tension, and friction force between water and cylinder surface. The restoring force and the friction force depends on many factors, such as the contacting surface roughness, and the size and density of the rivulet. The turbulent wind force and the aerodynamic damping force are also difficult to be quantified. For the sake of simplification, the combined effect of all damping forces on the rivulet is approximately represented by $-c|\dot{x}|^\alpha \dot{x}$. Here, \dot{x} is the relative velocity of the rivulet to the cylinder, which is equal to $R\dot{\theta}$; c is the damping coefficient of the rivulet; and α is a predetermined exponent. $\alpha=0$ represents a viscous damping force; $\alpha=1$ indicates the damping force from an orifice of square law. The restoring force due to water surface tension is assumed to be a linear function of the relative movement of the rivulet to the cylinder at this stage. The turbulence wind force is ignored since the size of the rivulet is small and the shape of the rivulet is naturally toward the streamline. Within all the above considerations, the dynamic equation of motion of the rivulet is expressed as

$$m\left(\ddot{\theta} + \frac{\ddot{y}\sin(\theta_o + \theta)}{R}\right) + c|\dot{\theta}|^\alpha \dot{\theta} + k\theta = 0 \quad (9)$$

where m , c , and k are the mass, damping coefficient, and stiffness coefficient per unit length of the rivulet. Eq. (7) to Eq. (9) can be combined and simplified as follows.

$$\begin{cases} \ddot{y} + 2\tilde{\xi}\omega_c\dot{y} + \omega_c^2 y = \tilde{F} \\ \ddot{\theta} + \frac{\ddot{y}\sin(\theta_o + \theta)}{R} + 2\xi_r\omega_r|\dot{\theta}|^\alpha \dot{\theta} + \omega_r^2\theta = 0 \end{cases} \quad (10)$$

in which

$$\tilde{\xi} = \xi_c + \xi_a; \quad \xi_a = \frac{\rho D \Gamma_2 U_o}{4M\omega_c}; \quad \tilde{F} = -\frac{\rho D}{2M}(\Gamma_1 R U_o \dot{\theta} + \Gamma_3 U_o^2 \theta) \quad (11)$$

where ξ_c and ξ_r denote the damping ratio of the cylinder and the rivulet, respectively; ξ_a is the aerodynamic damping ratio of the cylinder; $\tilde{\xi}$ is the total damping ratio; ω_c is the circular frequency of the cylinder in the y -direction; ω_r is the circular frequency of the rivulet; and \tilde{F} is the aerodynamic force acting on the cylinder in the y -direction due to the motion of rivulet. Since Γ_2 changes with the mean wind speed U_o through the static position of rivulet and depends on the motion of the cylinder and the rivulet, the aerodynamic damping ratio and hence the total damping ratio may be the function of time. Clearly, Eq. (10) is a strong nonlinear equation. The 4th order Runge-Kutta method can be applied to find the solution of motion for both the cylinder and the rivulet.

3. Comparison with test results

To investigate the capability of the 2DOF model for predicting the motion of inclined cylinder with moving rivulet, the inclined cylinder tested in a simulated wind-rain tunnel by Hikami and Shiraishi (1988) is selected for comparison. For the cylinder tested, the drag and lift coefficient curves of the cylinder with upper rivulet ($d/D=0.1$, d is the diameter of the rivulet) were reported by Yamaguchi (1990) and reproduced in Fig. 2. It is seen that there is a sudden change in the gradient of the curves around the angle of -55° . The curves are subsequently fitted to the Taylor's series of the first three terms distinguished by the critical angle of -55° . For the moving rivulet, its static position θ_o is the function of mean wind speed. The wind tunnel test results related to this position obtained by Hikami and Shiraishi (1988) are reproduced in Fig. 3 and fitted by a quadratic function. The inclined cylinder has the following parameters: the diameter is 140 mm; the mass per unit length is 10.2 kg/m; inclination and yawed angle are both 45° . The natural frequency of cylinder is 1 Hz. The structural damping ratio was not explicitly given in their paper for the test cylinder but a range of structural damping ratio from 0.0028 to 0.011 was provided for the cables in the prototype cable-stayed bridge. Therefore, an average value 0.007 of structural damping ratio is used in the comparison. The frequency of rivulet motion is taken as the same as that of cylinder motion, based on the observation from the simulated wind-rain tunnel tests by Hikami and Shiraishi (1988). The stagnation influence factor ε is selected as 0.4, by which the position of stagnation point is between the ideal angle of attack for the cylinder without rivulet and the ideal angle of attack for the cylinder without both rivulet and yaw angle. The two parameters related to the damping force on the rivulet, ξ_r and α , are set to be 10 and 1, respectively. This is because wind-rain-induced vibration occurs mainly on inclined cables with rough surface, that is, a high friction force between water and cylinder surface is expected due to a rough surface and high hydro-pressure in water rivulet. Nevertheless, the effects of ξ_r , α , and ω_r on the wind-rain-induced cylinder vibration will be investigated through parametric studies later on.

The results of the maximum displacement response amplitude of the cylinder obtained from the 2DOF model are displayed in Fig. 4 as the function of the mean wind speed U_o together with the wind tunnel test results. It is seen that the shape of the analytical curve is quite similar to that of the

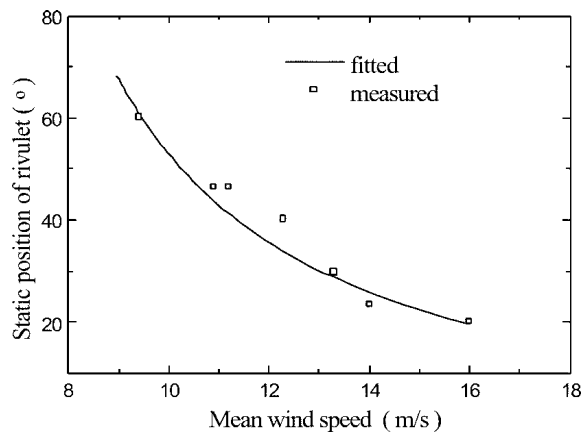


Fig. 3 Static position of upper rivulet vs. mean wind speed (Hikami and Shiraishi, 1988)

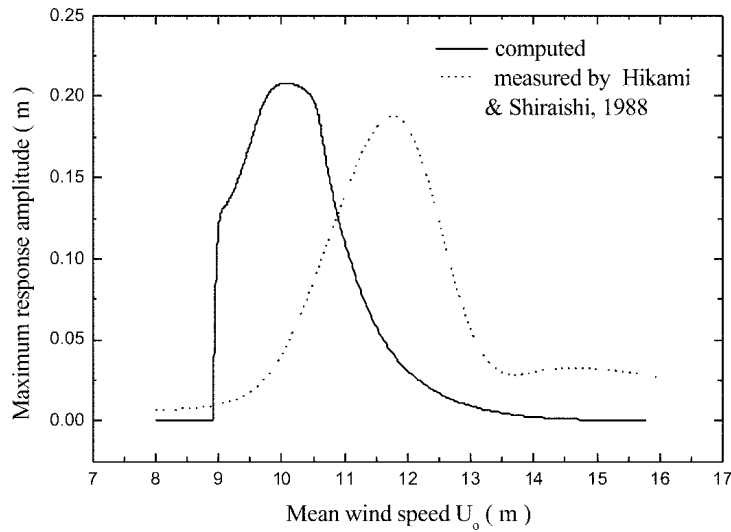


Fig. 4 Maximum cylinder vibration amplitude vs. mean wind speed

test curve. Both analytical and wind tunnel results show that wind-rain-induced cylinder vibration only occurs within a certain range of mean wind speed (the effective mean wind speed range). The wind-rain-induced cylinder vibration is a kind of vibration of restricted amplitude rather than galloping. The maximum displacement amplitude of the cylinder predicted by the 2DOF model is moderately larger than that measured from the wind-rain tunnel test. However, the predicted onset mean wind speed at which wind-rain-induced cylinder vibration starts to occur is lower than that measured from the wind-rain tunnel test. For the rivulet motion, the maximum angular displacement computed by the 2DOF model is 10° , occurring at the same time as the maximum displacement response of the cylinder. The maximum angular displacement of the rivulet of 10° is slightly lower than that of 12° measured from the wind-rain tunnel test. The predicted onset mean wind speed is about 8.7 m/s, which is also lower than 9.7 m/s from the wind-rain tunnel test. Such differences may be due to uncertainties in the selection of the parameters in the 2DOF model, such as the damping ratio of the rivulet ξ_r and the stagnation influence factor ε . Nevertheless, the 2DOF model does capture main vibration features of the inclined cylinder with the moving rivulet, such as velocity-restricted vibration and amplitude-restricted vibration.

4. Mechanisms of wind-rain-induced cable vibration

To investigate the possible mechanism behind wind-rain-induced cylinder vibration, the response time histories of the cylinder, the rivulet, and some key quantities are examined at the three particular mean wind speeds selected based on Fig. 4. The three mean wind speeds are selected at 9.1 m/s that corresponds to the cylinder vibration of medium level, at 9.8 m/s that corresponds to the cylinder global maximum vibration, and at 13 m/s at which the cylinder has very small vibration amplitude. All the parameters of the cylinder and the rivulet are kept the same as those used in the comparison with the test results.

At the mean wind speed of 9.8 m/s that is the critical mean wind speed, the computed time

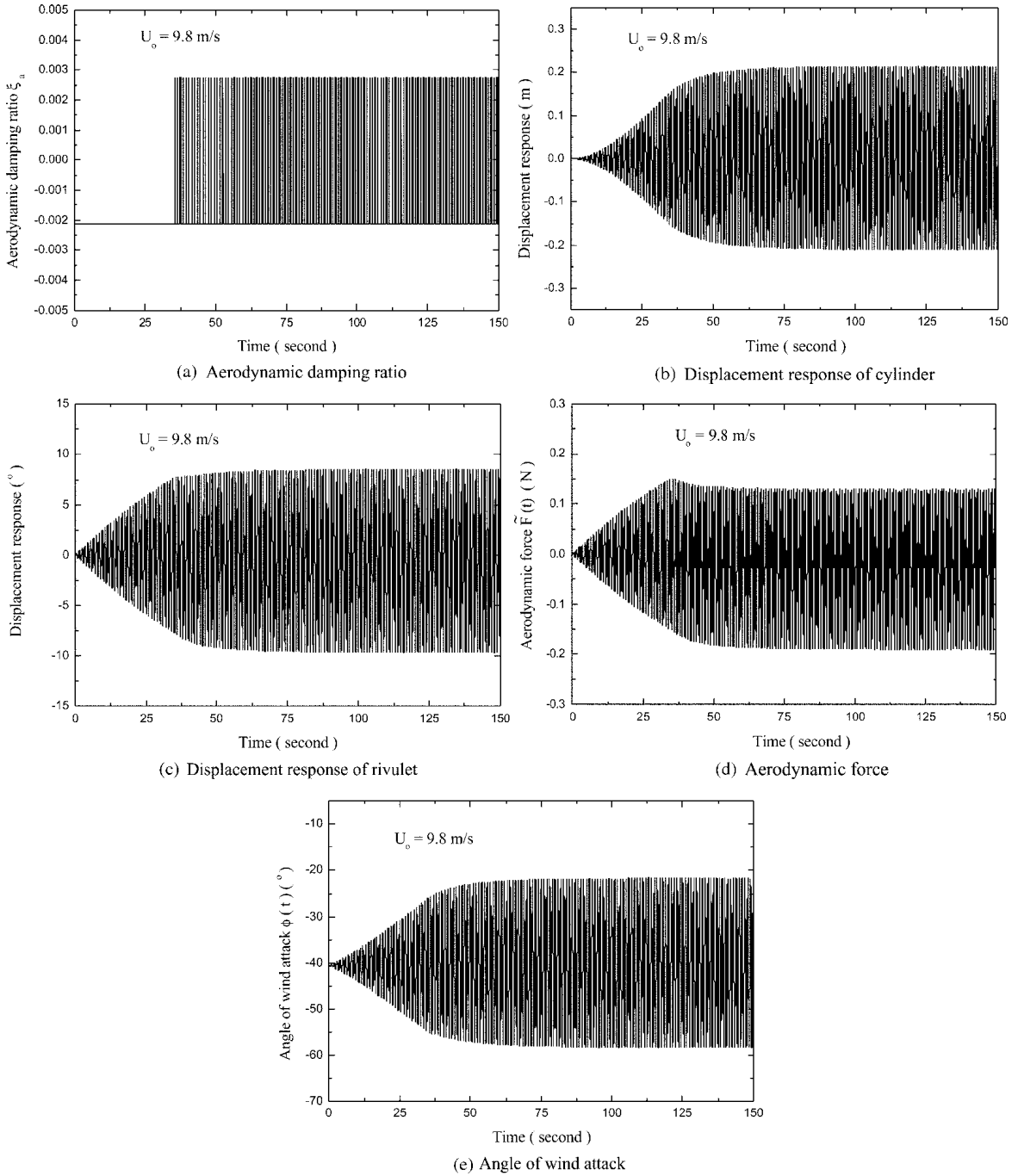


Fig. 5 Time histories of system vibration ($U_0 = 9.8$ m/s)

histories show that the aerodynamic damping ratio $\xi_a(t)$ is of constant negative value about -0.0021 during the first 35 seconds (see Fig. 5(a)). The total damping ratio therefore keeps the constant

value of 0.0049. The vibration amplitude of the cylinder increases from the initial zero displacement continuously because of the aerodynamic force caused by the motion of rivulet (see Fig. 5(b)). The rivulet is also oscillating together with the motion of the cylinder, and its amplitude increases with the increasing vibration amplitude of the cylinder (see Fig. 5(c)). As the rivulet vibration amplitude keeps increasing, the aerodynamic force $\tilde{F}(t)$ due to the rivulet motion increases with time (see Fig. 5(d)). Until the displacement amplitude of the cylinder and the angular displacement amplitude of rivulet $\theta(t)$ increase to a certain level, the angle of wind attack $\phi(t)$ reaches a stage where its negative amplitude becomes less than -55° , as shown in Fig. 5(e). Fig. 5(e) also shows that the initial angle of wind attack is about -40° , which depends on the mean wind speed. Consequently, the drag and lift coefficients of the cylinder with rivulet change their signs when the angle of wind attack $\phi(t)$ alters around -55° , as indicated in Fig. 2, and take two values only because of linearization used in the derivation of Eq. (7). Correspondingly, the aerodynamic damping ratio ξ_a and then the total damping ratio ξ no longer remain constant (see Fig. 5(a)), and the aerodynamic damping ratio alternates between the two values of -0.0021 and 0.0028 . Furthermore, the amplitude of aerodynamic force $\tilde{F}(t)$ becomes unsymmetrical because the gradients of the aerodynamic coefficient curves around the critical wind angle of -55° are unsymmetrical. As a result, when the aerodynamic damping ratio ξ_a is negative the vibration amplitudes of both the cylinder and the rivulet are enlarged. When the aerodynamic damping ratio ξ_a becomes positive, the further increase of vibration of both the cylinder and the rivulet is restrained. Since the negative aerodynamic damping ratio is small compared with the structural damping ratio in this case, the total damping ratio alternates between 0.0049 and 0.0098. Notwithstanding the total damping ratio is positive, it is quite small when the aerodynamic damping ratio is negative and the peak-to-peak amplitude of the aerodynamic force $\tilde{F}(t)$ due to the motion of rivulet is, however, relatively large. As a result, the cylinder exhibits a large but stable amplitude vibration (Fig. 5(b)). Thus, one may conclude that the existence of the rivulet is the main reason causing wind-rain-induced cable vibration in this case. On one hand, the rivulet motion inputs the energy into the system through the aerodynamic damping force associated with the negative aerodynamic damping ratio. On the other hand, the rivulet motion absorbs the energy from the system through the aerodynamic damping force associated with the positive aerodynamic damping ratio. This is why wind-rain-induced cylinder vibration in this case appears as a kind of amplitude-restricted vibration and also a kind of self-excited vibration.

At the mean wind speed of 9.1 m/s, the aerodynamic damping ratio $\xi_a(t)$ is -0.0072 in the first 10 seconds (see Fig. 6(a)). The total damping ratio is thus -0.0002 in the first 10 seconds. The vibration amplitudes of both the cylinder and the rivulet thus increase relatively fast with time until the angle of wind attack $\phi(t)$ reaches a stage where its negative amplitude becomes less than -55° . Afterwards, the aerodynamic damping ratio alternates between -0.0072 and 0.0079 , and the total damping ratio changes from -0.0002 to 0.0149 . The amplitude of aerodynamic force $\tilde{F}(t)$ is also unsymmetrical because the aerodynamic coefficient curves around the critical point of wind angle of attack are unsymmetrical (see Fig. 6(b)). However, the positive amplitude of the aerodynamic force is much smaller in this case than those at the mean wind speed of 9.8 m/s (see Fig. 5(d)). The reason is that the smaller mean wind speed in this case causes the initial angle of wind attack $\phi(t)$ around -50° , which is more close to the critical angle -55° . The larger positive total damping ratio and the smaller aerodynamic force make the vibration amplitude of the cylinder smaller in this case than the last case (see Fig. 6(c)). It is noted from this case that the small negative damping ratio does not induce the instability of the cylinder vibration. The reason is that the negative value of the

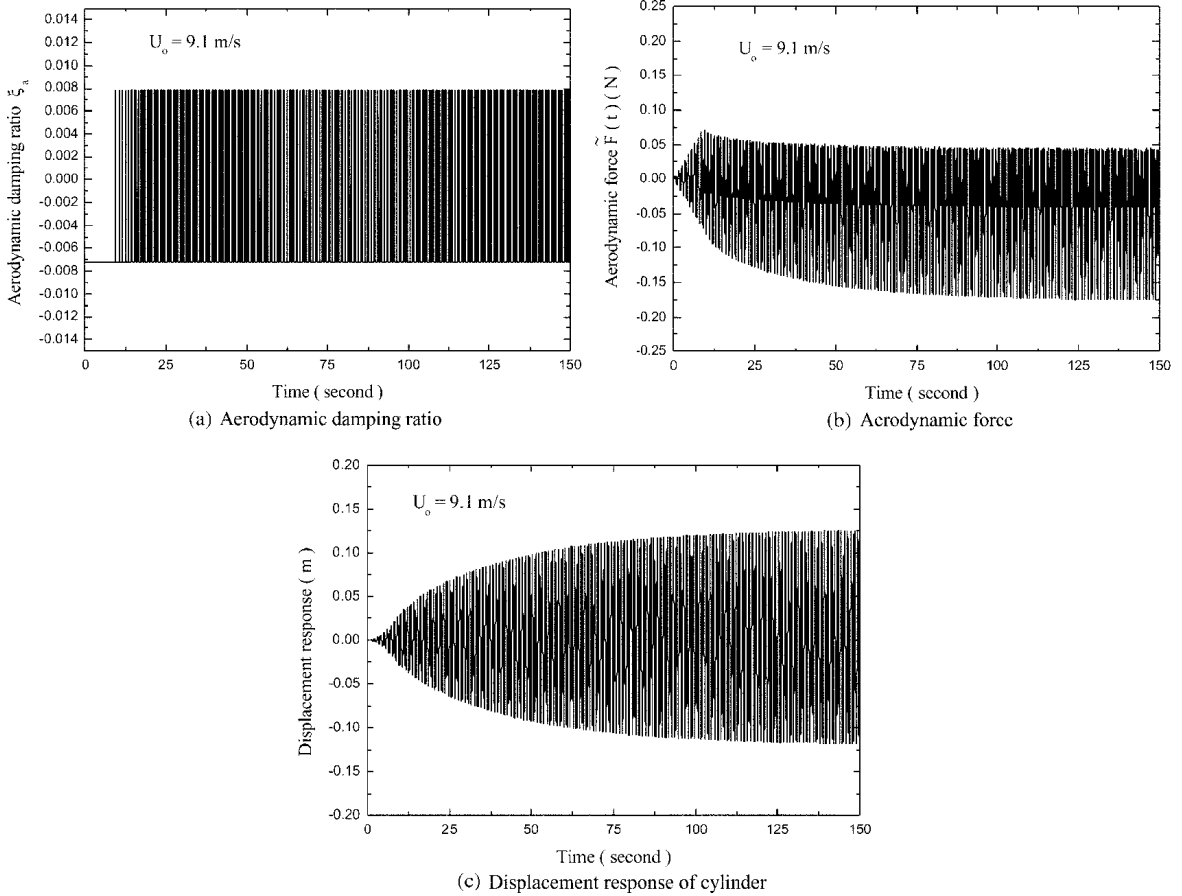


Fig. 6 Time histories of system vibration ($U_0 = 9.1$ m/s)

total damping ratio and the positive value of the total damping ratio both appear in one vibration cycle. The motion of the rivulet excites on one hand and depresses on the other hand the vibration of the cylinder. It seems that the effect of aerodynamic damping ratio is more complicated in wind-rain-induced cable vibration than other wind-induced cable vibrations.

At the mean wind speed of 13 m/s, the aerodynamic damping ratio ξ_a is of positive value about 0.01 and remains constant all the time (see Fig. 7(a)). The total damping ratio is then of constant positive value about 0.017. Therefore, the existence of the rivulet dampens the vibration of the cylinder in this case. However, the motion of the rivulet generates the aerodynamic force $\tilde{F}(t)$ to excite the cylinder in the y -direction (see Fig. 7(b)). When the energy input by the aerodynamic force $\tilde{F}(t)$ is balanced by the energy exhausted by the aerodynamic damping and system structural damping, the cylinder exhibits a stable vibration of very small amplitude (see Fig. 7(c)). Since the aerodynamic damping ratio keeps a positive constant value, the aerodynamic force is symmetrical in this case. The mechanism of the cylinder and rivulet vibrations somewhat likes vortex shedding induced cylinder vibration. This case also indicates that the motion of rivulet can induce cylinder vibration even if there is no negative aerodynamic damping.

From the above three cases, it is seen that wind-rain-induced cylinder vibration may have different

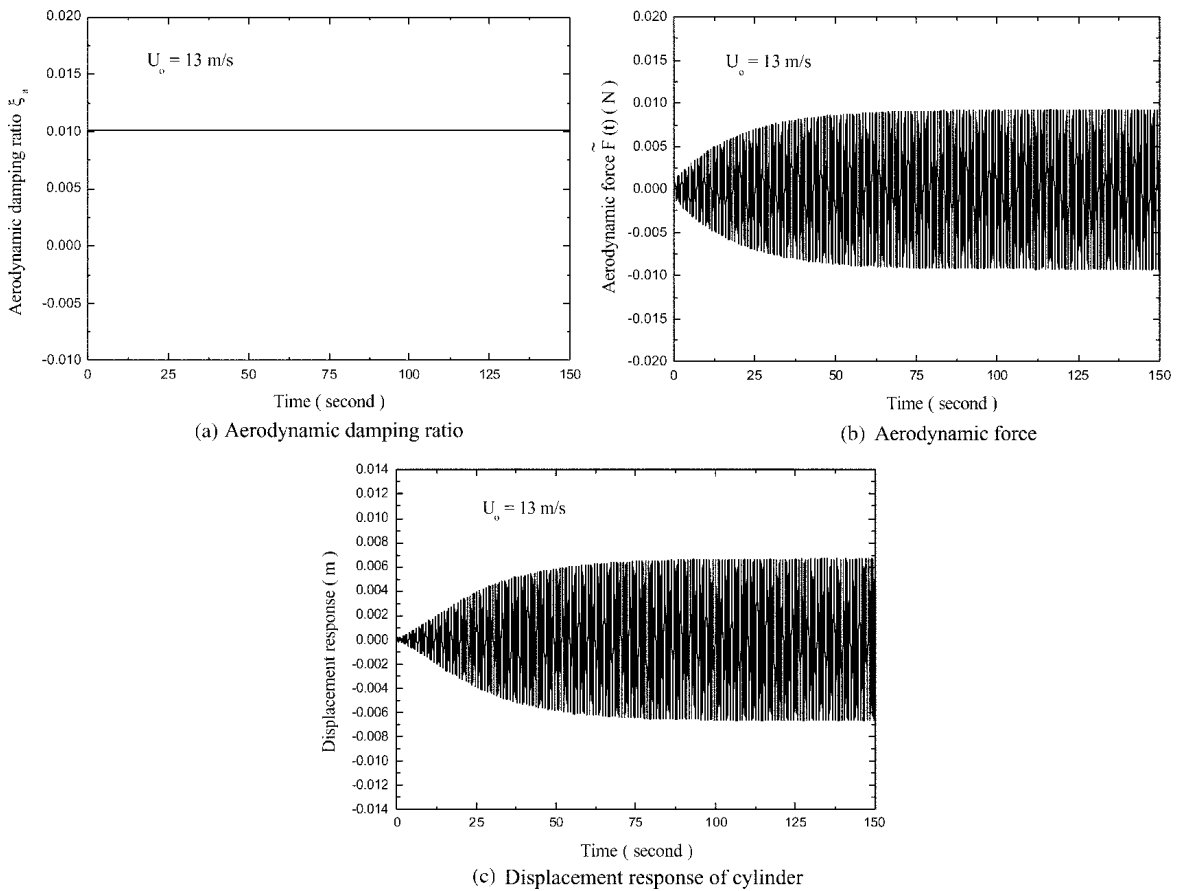


Fig. 7 Time histories of system vibration ($U_o = 13$ m/s)

mechanisms. The existence of the rivulet has two possible effects: one generates the negative aerodynamic damping that induces large amplitude cylinder vibration; the other produces the positive aerodynamic damping that reduces the cylinder vibration. The motion of the rivulet also generates the aerodynamic force on the cylinder to excite the cylinder to vibrate. The occurrences of which type of wind-rain-induced cylinder vibration depends on the mean wind speed and the static position of rivulet. The aforementioned results are consistent with the view of point of Ruscheweyh (1999) that the rhythmic movement of the rivulet is the “trigger” for starting wind-rain-induced cable vibration. They also coincide with the early reports from Matsumoto *et al.* (1992) that aerodynamic stabilization could be attained through rivulet installation at a certain position. Some other reports (Matsumoto *et al.* 1995, Bosdogianni and Olivari 1996) emphasize that the position of the rivulet plays an important role in the cable of aerodynamically unstable cross section.

5. Parametric studies

There are three parameters involved in the equation of motion of the rivulet; the damping ratio ξ_r , the damping exponent α , and the circular frequency ω_r . These parameters cannot be experimentally

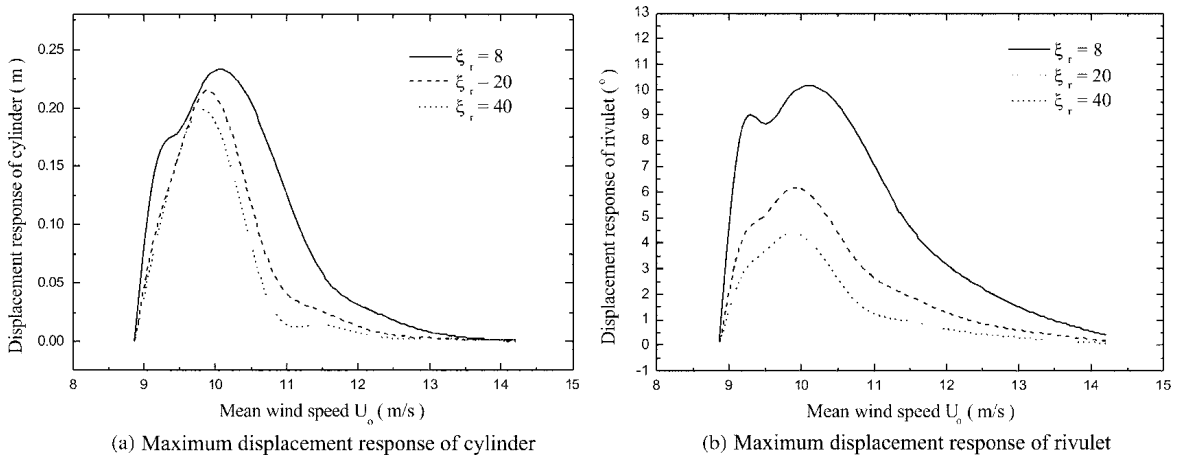


Fig. 8 Effects of rivulet damping ratio

determined at this stage. Thus, parametric studies are needed to see how sensitive the cylinder motion is to these parameters so that a reasonable judgment can be made on the aforementioned computed results.

Let us first consider the damping ratio of the rivulet ζ_r . While all the other parameters of the cylinder and the rivulet are kept the same as in the previous sections, the damping ratio of the rivulet is taken as a variable. The computed maximum displacement response of the cylinder and the maximum angular displacement response of the rivulet are displayed in Figs. 8(a) and 8(b), respectively, against the mean wind speed for three different damping ratios. It is seen that the increase of the damping ratio of rivulet narrows the effective mean wind speed range. It also reduces the cylinder motion to some extent. However, the reduction of the global maximum displacement response of the cylinder around the critical mean wind speed is not significantly. The increase of damping ratio from 8 to 40 yields a reduction of the global maximum displacement response of the cylinder from 0.23 m to 0.20 m only. The increase of damping ratio, however, leads to a significant decrease of the global maximum angular displacement response of the rivulet from about 10 $^\circ$ to 4.3 $^\circ$. Thus, from a practical point of view one may conclude that the maximum motion of cylinder is not very sensitive to the damping ratio of rivulet in this study.

The second parameter considered is the damping exponent α . The effects of the damping exponent on the maximum displacement responses of both the cylinder and the rivulet are shown in Figs. 9(a) and 9(b), respectively. The smaller exponent makes the effective mean wind speed range narrower but only moderately reduces the global maximum displacement of the cylinder. The increase of the exponent from 0.5 to 2.0 yields an increase of the global maximum displacement of the cylinder from 0.21 m to 0.24 only. However, the increase of the exponent from 0.5 to 2.0 leads to an increase of the global maximum angular displacement of the rivulet from 8.7 $^\circ$ to 12.5 $^\circ$. Again, from a practical point of view the maximum motion of cylinder is not very sensitive to the damping exponent in this study.

The third parameter considered in this study is the circular frequency of the rivulet ω_r . Figs. 10(a) and 10(b) show the variations of the maximum displacement response of the cylinder and the maximum angular displacement response of the rivulet with the mean wind speed for three different frequency ratios $\omega_r/\omega_c = 0.75, 1.00, \text{ and } 1.20$. For the frequency ratios concerned, the change of the

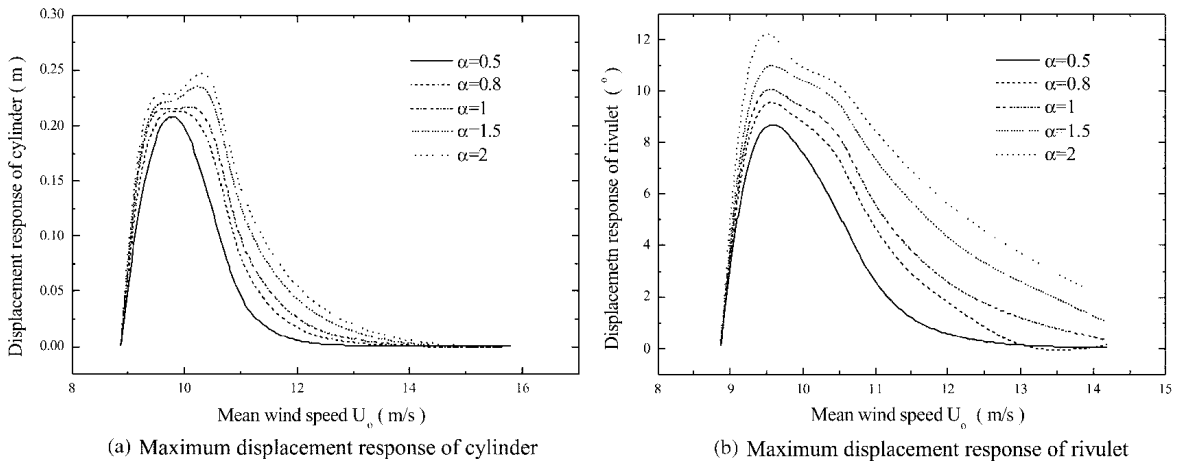


Fig. 9 Effects of rivulet damping exponent

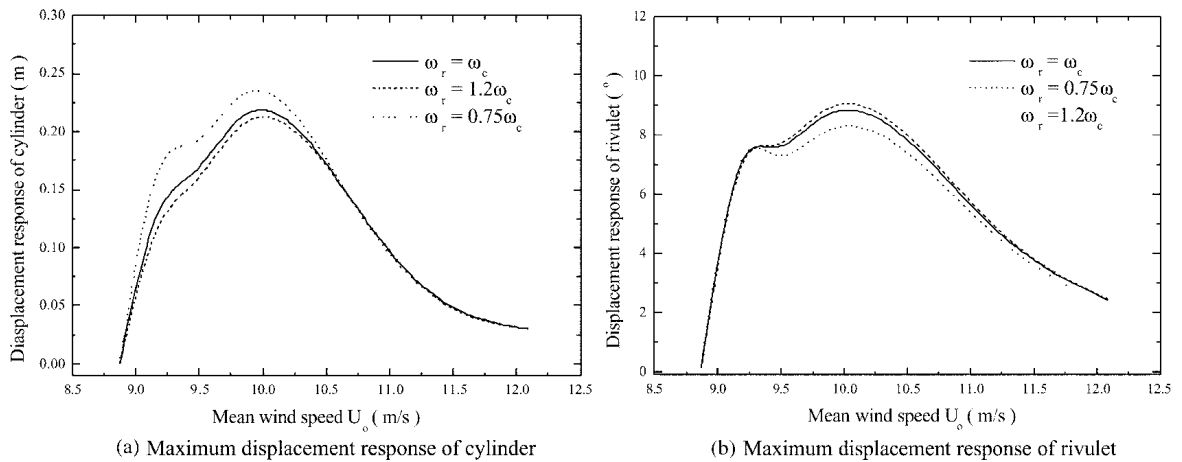


Fig. 10 Effects of rivulet frequency

frequency of the rivulet only slightly affects the maximum displacement responses of both the cylinder and the rivulet. There is only a smaller reduction of the maximum displacement responses of both the cylinder and the rivulet for a larger rivulet frequency.

The last parameter considered here is the structural damping ratio of the cylinder. Though the mechanism of wind-rain-induced cable vibration is not clear, some mechanical devices such as oil dampers have been already installed on the stay cables near the cable anchorages in some cable-stayed bridges with the purpose of increasing the structural damping to mitigate the vibration (Xu, Zhan, Ko and Yu 1999). Therefore, it is interesting to know if the 2DOF model can capture this trend. In this regard, the structural damping ratio ξ_a of the inclined cylinder is taken as a variable while all the other parameters remain unchanged. The maximum displacement response of the cylinder and the maximum angular displacement response of the rivulet are computed for the structural damping ratios of 0.005, 0.007, and 0.010 and for a series of mean wind speeds. The computed results are plotted in Figs. 11(a) and 11(b) accordingly. It is seen from Fig. 11(a) that the increase of structural

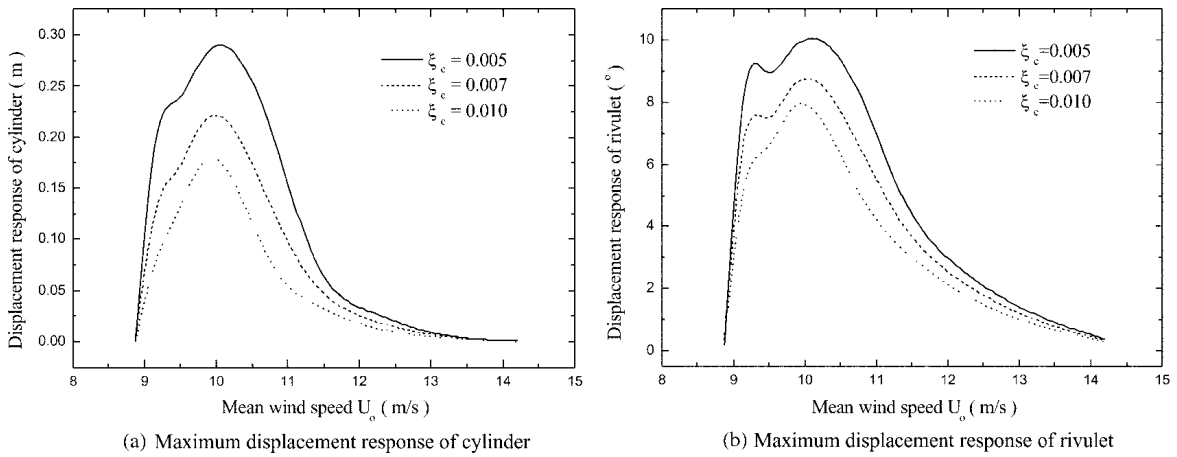


Fig. 11 Effects of cylinder damping ratio

damping ratio can significantly reduce wind-rain-induced cylinder vibration around the critical mean wind speed. The increase of structural damping ratio from 0.005 to 0.010 leads to a decrease of the global maximum displacement response of the cylinder from 0.29 m to 0.18 m. The increase of structural damping ratio also narrows the effective mean wind speed range. Though the maximum angular displacement response of rivulet also decreases with the increase of structural damping ratio, the decreasing rate is much smaller than that of the cylinder. It can thus be concluded that the increase of structural damping can effectively suppress the cylinder motion but moderately reduce the rivulet motion.

6. Comparison with SDOF model

As mentioned before, in the SDOF model the governing equation of motion of wind-rain-induced cylinder vibration is obtained by quantifying the rivulet motion using the measured results reported by Hikami and Shiraishi (1988). It is assumed that the rivulet motion is harmonic motion with a given amplitude. In the 2DOF model, this assumption is released. Fig. 12 displays the maximum displacement response of the cylinder against mean wind speed obtained by both the SDOF model and the 2DOF model. The parameters of the cylinder are the same for both the computed cases. It is seen from Fig. 12 that at very low and high mean wind speeds, the vibration amplitude of the cylinder predicted by the SDOF model is larger than that predicted by the 2DOF model. Within the range around the critical mean wind speed, the vibration amplitude of the cylinder predicted by the 2DOF model is larger than that computed by the SDOF model in general. What is more, the computed curve of vibration amplitude of the cylinder by the 2DOF model is closer to the measured results than that computed from the SDOF model. It is thus concluded that the two-degree-of-freedom model is a better model to predict and explain the phenomena and mechanism of wind-rain-induced cable vibration than the single-degree-of-freedom model. However, the single-degree-of-freedom model is also acceptable to obtain the global maximum vibration response of the cylinder in consideration of its simplicity.

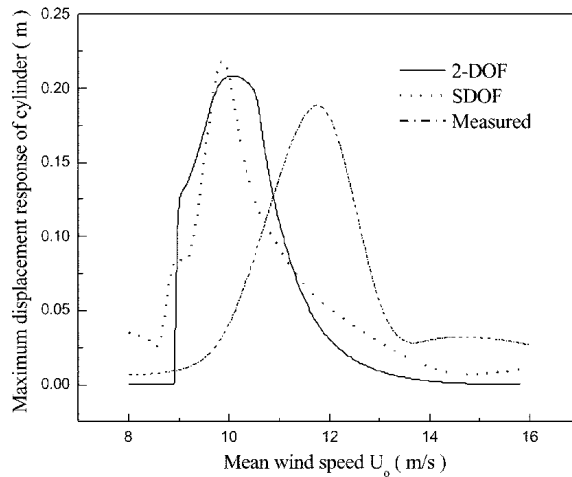


Fig. 12 Comparison between 2DOF model and SDOF model

7. Conclusions

A two-degree-of-freedom (2DOF) model for describing wind-rain-induced cable vibration has been proposed in this paper. The analytical model was verified through the comparison with the wind-rain tunnel test results, and the comparison was found satisfactory in general. The inherent mechanisms of wind-rain-induced cylinder vibration were then investigated by employing the 2DOF analytical model. It was found that the 2DOF model is able to capture the main vibration features of the inclined cylinder with upper rivulet, such as velocity-restricted vibration and amplitude-restricted vibration. The occurrence of velocity- and amplitude- restricted vibration is mainly because of alternating aerodynamic damping ratio and/or alternating excitation force due to the interaction between rivulet motion, cable motion and wind. It was also found that the mechanism of wind-rain-induced cylinder vibration depends on the mean wind speed and the static position of the upper rivulet. The parametric study also indicated that the damping ratio and exponent of the rivulet affect the maximum response of cylinder moderately, and the frequency of the rivulet only slightly influences the cylinder motion. The 2DOF model is better than the SDOF model to predict and explain the phenomena and mechanism of wind-rain-induced cable vibration but the SDOF model is also applicable and has advantage of its simplicity.

It should be pointed out that in the derivation of wind-rain-induced aerodynamic force on the cylinder, the effects of axial flow and turbulence are not considered in this investigation because there are no enough information and knowledge for the writers to quantify their effects, which needs further investigation.

Acknowledgements

The writers are grateful for the financial support from the Research Grants Council of Hong Kong through a CERG Central Allocation Vote.

References

- Bosdogianni, A. and Oliver, D. (1996), "Wind and rain induced oscillations of cables of stayed bridges", *J. Wind Eng. Ind. Aerodyn.*, **64**, 171-185.
- Geurts, C.P.W. and van Staaldouin, P.C. (1999), "Estimation of the effects of rain-wind-induced vibration in the design stage of inclined stay cables", *Proc. of 10th Int. Conf. on Wind Eng.*, Denmark, Balkema, Rotterdam, **2**, 885-892.
- Hikami, Y. and Shiraishi, N. (1988), "Rain-wind induced vibrations of cables in cable stayed bridges", *J. Wind Eng. Ind. Aerodyn.*, **29**, 409-418.
- Matsumoto, M., Shiraishi, N., and Shirato, H. (1992), "Rain-wind induced vibration of cables of cable-stayed bridges", *J. Wind Eng. Ind. Aerodyn.*, **41-44**, 2011-2022.
- Matsumoto, M., Yamagishi, M., Aoki, J., and Shiraishi, N. (1995), "Various mechanism of inclined cable aerodynamics," *Proc. of 9th Int. Conf. on Wind Eng.*, Wiley Eastern, New Delhi, **2**, 759-769.
- Matsumoto, M., Yagi, T., Shigemura, Y., and Tsushima, D. (2001), "Vortex-induced cable vibration of cable-stayed bridges at high reduced wind velocity", *J. Wind Eng. Ind. Aerodyn.*, **89**, 633-647.
- Matsumoto, M., Yagi, T., Shirato, H., Sakai, S., Ohya, J., and Okada, T. (2003), "Field observations of wind-induced cable vibrations using large scale inclined cable model", *Proc. of 11th Int. Conf. on Wind Eng.*, Lubbock, Texas, USA, **2**, 2149-2156.
- Ruscheweyh, H.P. (1999), "The mechanism of rain-wind induced vibration", *Proc. of 10th Int. Conf. on Wind Eng.*, Denmark, Balkema, Rotterdam, **2**, 1041-1047.
- Xu, Y.L., Zhan, S., Ko, J.M., and Yu, Z. (1999), "Experimental study of vibratiav mitigation of brdige stay cables", *J. Struct. Eng.*, ASCE, **125**(9), 977-986.
- Xu, Y.L. and Wang, L.Y. (2003), "Analytical study of wind-rain-induced cable vibration: SDOF model", *J. Wind Eng. Ind. Aerodyn.*, **91**, 27-40.
- Yamaguchi, H. (1990), "Analytical study on growth mechanism of rain vibration of cables", *J. Wind Eng. Ind. Aerodyn.*, **33**, 73-80.
- Zuo, D.L. and Jones, N.P. (2003), "Interpretation of observed damper performance in mitigating wind and rain-wind induced stay-cable vibrations", *Proc. of 11th Int. Conf. on Wind Eng.*, Lubbock, Texas, USA, **2**, 2133-2140.